

# Remote dynamic actuation of an electrostatically driven microcantilever by a wireless power transfer system

Raul Ruiz <sup>\*</sup>, Gabriel Abadal

Dept. Enginyeria Electrònica, Campus UAB, 08193 Bellaterra, Spain



## ARTICLE INFO

**Keywords:**  
RF-MEMS  
Wireless power transfer  
Electrostatic actuation

## ABSTRACT

The design, modelling, fabrication and test of a device prototype, based on a microcantilever capacitively connected to a folded-end half-wave dipole antenna, which is remotely actuated by a wireless power transfer (WPT) system are presented here. The microcantilever and the antenna, which are coupled at the antenna feeding point, work as a new device, is able to harness the radiated energy wirelessly transferred from an emitter antenna to directly excite the mechanical vibration modes of the microcantilever. The response to an amplitude-modulated (AM) RF radiated signal excitation produced by a transmitting antenna is experimentally analysed and fit to a simple model when the distance between both antennas varies from the near field to the radiated far field regime.

## 1. Introduction

Since Nicola Tesla's patent, the system of transmission of electrical energy [1] and the experiments of H. Yagi and S. Uda in wireless power transfer WPT [2], multiple advances have been made in subsequent years, mainly due to progress in wireless technology and architectures. Currently, applications on non-radiative or radiative field WPT range from medical implants [3,4], consumer electronics [5,6], wireless sensor networks (WSN) [7], electric vehicles [8], internet of things (IoT) [9], among others. These applications normally require converting the energy previously captured before being used by means of a rectenna (rectifying antenna) [10], which in combination with a voltage doubler and a charge pump converts RF signals to direct current (DC). The efficiency of rectenna-based WPTs depends on all the components involved [11].

In addition, the RF-MEMS technology has evolved, and MEMS have played an important role as passive components in RF-switches [12], where they have reached frequency ranges from DC to 120 GHz in oscillators [13], filters [14] and the reconfiguration of antennas working at frequency ranges of 12–200 GHz. MEMS with electrostatic actuation, have been particularly used as components of integrated AM-FM demodulation systems, replacing the conventional mixer circuit in heterodyne communication receivers by a mechanical mixer [15], reducing size, cost and power consumption of the traditional mixer blocks. The second order nonlinear relationship between the electrostatic force and

the voltage is the base of operation of mechanical mixers. With the advance in MEMS technologies, new devices with high Q-factors made it possible to design filters and combine both functionalities, mixing and filtering, in a single device named mixler [16]. RF demodulation has been also used in an homodyne receiver [17], where the electrostatic actuator is driven by a resonant circuit [18] consisting of a resistance and an inductance that together with the capacitance of the electrostatic actuator form an RLC circuit, whose resonant frequency is selected to be equal to the carrier frequency of the RF signal. Complex cascade MEMS architectures have been designed recently [19] to expand the power handling capability of direct amplitude demodulators, which is a key requirement for 5 G applications. However, all previously mentioned RF-MEMS solutions can replace and improve the performance of only some of the blocks of a radio receiver circuitry. Other blocks such as the low noise amplifier (LNA) or even the antenna are still implemented by standard components.

A wise and disruptive proposal was made in the past [20] to integrate, in a NEMS structure - based on a single carbon nanotube -, all the components except for the speaker of a 40–400 MHz radio receiver: antenna, tunable band-pass filter, amplifier, and demodulator. Nonetheless, a DC voltage source was needed to power the nanotube radio and even the antenna needed to be polarized to perform its functionality.

In a previous work, we demonstrated the operation in reception of a fully passive mechanical antenna based on a microcantilever with a permanent charge implanted, which directly interacted with the electric

<sup>\*</sup> Corresponding author.

E-mail address: [raul.ruizl@autonoma.cat](mailto:raul.ruizl@autonoma.cat) (R. Ruiz).

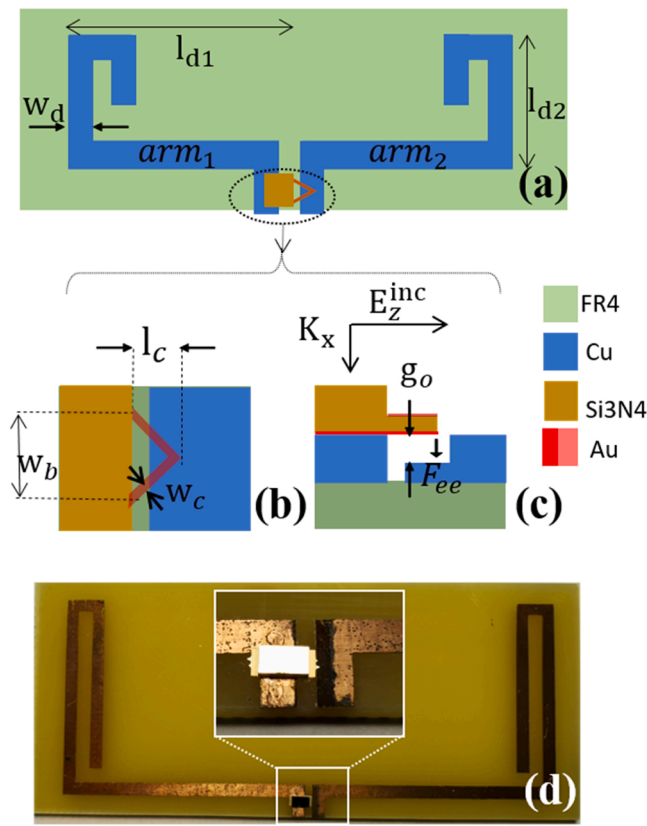


**Fig. 1.** Layout of the MEMSTENNA. Top view of the dipole antenna with the cantilever coupled into its feeding point (a). Detail of the top V-shaped microcantilever (b) and lateral cross section with a local thickness reduction on  $arm_2$  allowing to define a vertical capacitive gap,  $g_o$ , for the electrostatic excitation of the cantilever (c). Top view photograph of the MEMSTENNA prototype with a detail of the microcantilever in the feeding point region (d).

field of a RF radiation [21]. Although such MEMS antenna entailed a huge miniaturization, it operated at 11 kHz, which is a frequency far from the GHz bands of the modern application trends. Recently, we proposed a new device called MEMSTENNA [22], which combines the radiation absorption functionality of the antenna with the AM demodulation, filtering and mechanical actuation capabilities of a capacitive MEMS. Such a MEMSTENNA transduces the electromagnetic power radiated by a transmitter antenna directly to a static or dynamic mechanical actuation of the microcantilever. The same transduction mechanism has been described previously in an optomechanical THz detector [23]. The working principle, DC operation and preliminary results of AC operation in the near field regime have been recently reported [24]. A MEMSTENNA functioning as a wireless switch has a field of application in wake-up radio receiver architectures [25–27] where one of the objectives is to minimize power consumption.

In this paper, we present an equivalent circuit model of the MEMSTENNA that describes the electromechanical dynamics of the device and predicts its response to an AM-modulated signal excitation. Experimental results of this response in the far-field regime obtained from the characterization of a test prototype and fit to the model predictions are also presented.

## 2. MEMSTENNA prototype and equivalent circuit model

Our MEMSTENNA test prototype is based on a folded-end half-wave dipole antenna designed from a resonance frequency specification at 0.8 GHz on a Cu-FR4 substrate (Fig. 1a) and a commercial silicon nitride microcantilever [28] with Au coating (70 nm top / 35 nm bottom) and a thickness of  $t_c = 600$  nm with a spring constant of 0.08 N/m and

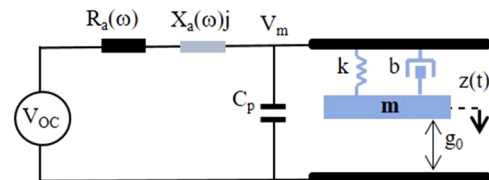


**Fig. 2.** Thévenin equivalent circuit of the MEMSTENNA as a dipole antenna (left side) loaded by the capacitance  $C_m$  of the MEMS capacitive actuator (right side), represented by its spring ( $k$ ) mass ( $m$ ) damper ( $b$ ) model and a parasitic capacitance  $C_p$ .

**Table 1**

Datasheet of the MEMSTENNA prototype.

Parameter	Value	Units
Dipole arm length ( $l_{d1}/l_{d2}$ )	35/30	mm
Dipole width ( $w_d$ )	2	mm
Dipole thickness ( $t_d$ )	35	μm
Cantilever length ( $l_c$ )	200	μm
Cantilever width ( $w_c$ )	28	μm
Cantilever base width ( $w_b$ )	184	μm
Cantilever spring constant ( $k_c$ )	0.08	N/m
Cantilever thickness, Si <sub>3</sub> N <sub>4</sub> ( $t_c$ )	0.6	μm
Capacitive gap ( $g_o$ )	34	μm
Overlapping Area (A)	162	μm <sup>2</sup>
Dipole resonant frequency ( $f_d$ ):		
measured/simulated	0.88/0.82	GHz
Cantilever resonant frequency ( $f_c$ )	17	kHz

resonance frequency at 17 kHz, as it can be observed in Fig. 1b and c. The folded-end dipole antenna consists of two arms ( $arm_1$  and  $arm_2$ ) of length  $\lambda/4$  each separated by a gap which corresponds to the feeding point of the antenna. The triangular microcantilever, composed of two clamped-free microbeams parallelly connected in a V-shaped configuration, is placed at the feeding point of the dipole as it is sketched in Fig. 1: the microcantilever is turned upside down so that its clamping support is electrically contacted to  $arm_1$  through its conductive surface. Its free end stays parallelly placed on top of  $arm_2$  along an overlap area,  $A=162\text{ }\mu\text{m}^2$  and separated by a gap,  $g_o=34\text{ }\mu\text{m}$ . The gap is defined by the local Cu thickness reduction of  $arm_2$  (Fig. 2c). The dimensions of the antenna and the microcantilever are reported in Table 1.

It can be noticed that from an electrical point of view, the microcantilever placed as described above implies a capacitive load for the antenna with a capacitance described by Eq. (1):

$$C_m = \frac{\epsilon_0 \cdot A}{2 \cdot g_o} \quad (1)$$

When the dipole antenna is excited by the electric field,  $E_z^{inc}$  of a radiated electromagnetic plane wave (see Fig. 1.c), a voltage is generated at the feeding point of the antenna. In open circuit conditions it is denoted by  $V_{oc}$  and called open circuit voltage. The relationship between the electric field and the induced voltage in the antenna is a parameter of the antenna called antenna factor AF [29]:

$$V_{oc} = \frac{E_z^{inc}}{AF} \quad (2)$$

The antenna factor is defined in Eq. (3) as:

$$AF = \sqrt{\frac{4\pi \cdot \eta \cdot f^2}{c^2 \cdot G \cdot Z_{load}}} \quad (3)$$

Where  $\eta$  is the intrinsic impedance of the free space, approximately 377 Ω,  $c$  is the speed of light,  $f$  is the frequency of the plane wave,  $Z_{load}$  is the impedance of the antenna load and  $G$  is the gain of the antenna. As indicated in the equivalent circuit of Fig. 2,  $V_{oc}$ , generated by the incidence of the electric field in the dipole, is distributed between the

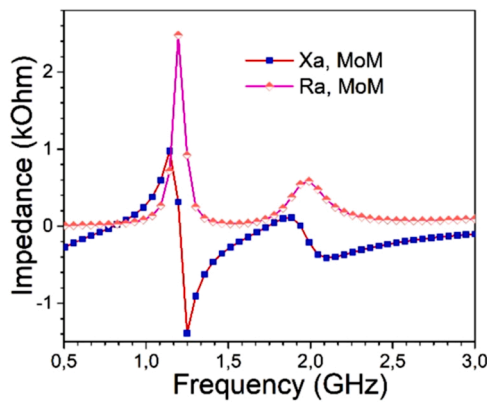


**Fig. 3.** Frequency response of the MEMSTENNA dipole impedance components obtained with the method of moments (MoM).

impedance of the antenna  $Z_a = R_a + jZ_a$  and the impedance of the capacitive load produced by the microcantilever  $Z_{load} = -j/wC_m$ , as described in Eq. (1). The voltage drop in the cantilever,  $V_m$ , induces an electrostatic force:

$$F_{ee} = \frac{\epsilon_0 \cdot A \cdot V_m^2}{2 \cdot (g_0 - z(t))^2} \quad (4)$$

which, as depicted in Fig. 1.c, acts on the microcantilever and produces its vertical displacement  $z(t)$ , as represented in Fig. 2. The nonlinearity of the electrostatic force [30], due to its inversely squared dependence on the displacement,  $z$ , but especially because of its quadratic dependence on the voltage  $V_m$ , will play a crucial role on the transducing mechanism of the MEMSTENNA in the dynamical regime as will be described below. The complex dynamics involved by the non-linear dependence of the excitation force on the free-end cantilever position over time,  $z(t)$ , is described by the MEMSTENNA model represented in Fig. 2.

The MEMSTENNA dipole antenna part, which is a receiving antenna, is electrically modelled by its Thévenin equivalent circuit, as shown in Fig. 2.

The values of the components of the antenna dipole impedance, resistance  $R_a$  and reactance  $X_a$ , in the frequency interval between 400 MHz and 2.5 GHz are calculated by the method of moments (MoM) and represented in Fig. 3.

Moreover, the electromechanical model of the microcantilever capacitive actuator is based on a spring-mass-damper system. The movement Eq. (5) describes the dynamic behaviour of the microcantilever:

$$m \cdot \frac{d^2z(t)}{dt^2} + b \cdot \frac{dz(t)}{dt} + k \cdot z(t) = F_{ee}(t) \quad (5)$$

where  $m$  is the effective mass,  $k$  is the spring constant and  $b$  is the damping factor. The deflection of the beam, in terms of the displacement of the cantilever free end, is represented by  $z(t)$ .  $F_{ee}$  represents the electrostatic force as defined in Eq. (4). Eq. (5) can be rewritten as Eq. (6) by replacing  $F_{ee}$  by its explicit form (4):

$$m \cdot \frac{d^2z(t)}{dt^2} + b \cdot \frac{dz(t)}{dt} + k \cdot z(t) = \frac{\epsilon_0 \cdot A \cdot V_m^2(t)}{2 \cdot (g_0 - z(t))^2} \quad (6)$$

When the dipole is excited by a carrier signal of frequency  $f_c = 531-571$  MHz, the impedance of the antenna is capacitive as Fig. 3 shows, then the dynamic behaviour of the dipole circuit is described by Eq. (7):

$$R_a \cdot \frac{dq(t)}{dt} + \frac{q(t)}{C_{tt}} = V_{oc}(t) \quad (7)$$

Here,  $q$  is the electric charge and  $C_{tt}$  is the total equivalent capacitance of the MEMSTENNA, obtained by connecting the antenna capacitance,  $C_a$ , in series with the total microcantilever load capacitance,  $C_{mt}$ , as defined by:

$$C_{mt} = C_m(g(t)) + C_p \quad (8)$$

$$C_{tt} = (C_{mt} \bullet C_a) / (C_{mt} + C_a) \quad (9)$$

where  $C_{mt}$  includes a parallel parasitic capacitance,  $C_p$ , which describes the static capacitive coupling between the two arms of the dipole and the clamping support of the microcantilever.

When the MEMSTENNA is excited by an amplitude-modulated radio frequency signal (AM), the voltage at the terminals of the microcantilever is defined as (10):

$$V_m(t) = |V_m| \cdot [1 + m \cdot A_m \cdot \sin(\omega_m \cdot t)] \cdot \sin(\omega_c \cdot t) \quad (10)$$

where  $m$  is the modulation index ( $m \leq 1$ ),  $A_m$  is the modulating amplitude,  $\omega_c$  is the carrier frequency and  $\omega_m$  is the modulating frequency. If the voltage expression of Eq. (10) is introduced in the force Eq. (4) and if

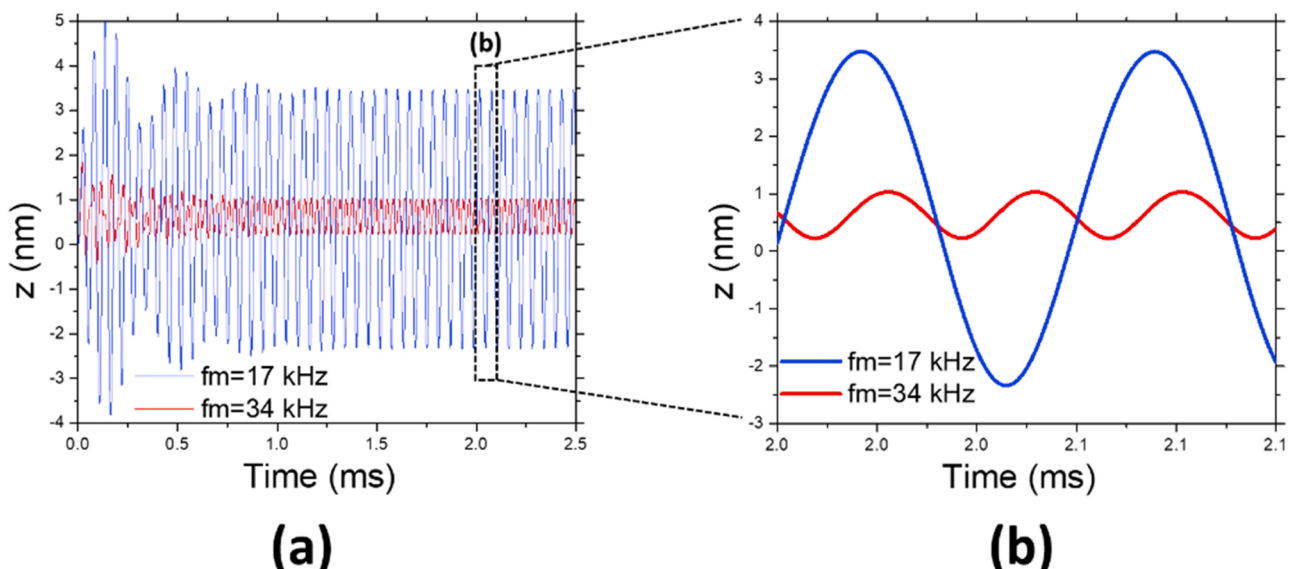


**Fig. 4.** Calculated cantilever free-end displacement corresponding to the demodulated signal at frequency  $f_m = 17$  kHz and  $f_m = 34$  kHz with modulation index = 0.8.

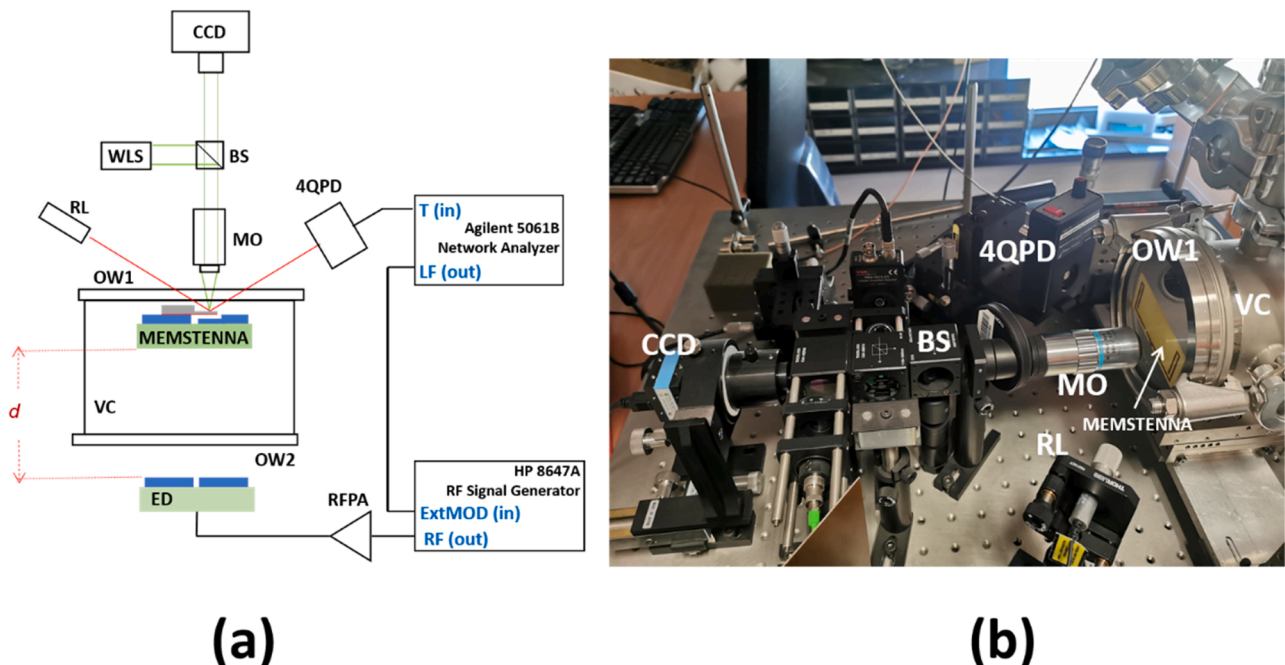


**Fig. 5.** Diagram (a) and general view photograph of the test setup (b). Used components: CCD: Digital camera, BS: Beam Splitter, WLS: White Light Source, 4QPD: 4-Quadrants Photodetector, MO: Microscope Objective (50X), OW1: Optical Window, OW2: Optical Window, RFPA: RF Power Amplifier (2 W), ED: Emitter Dipole, RL: Red Laser ( $\lambda = 673.8$  nm), VC: Vacuum Chamber.

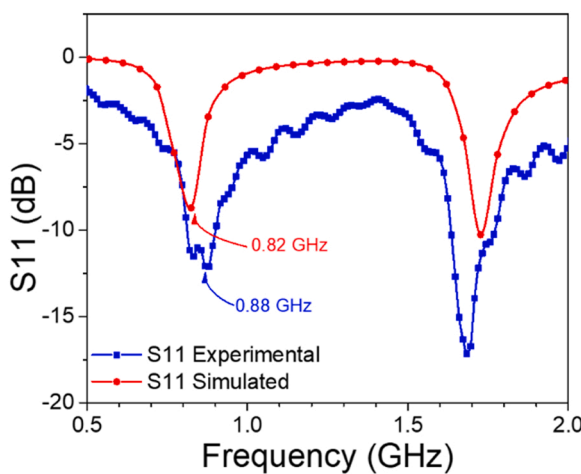


**Fig. 6.** Measured and MATLAB simulated S11 parameter of the MEMSTENNA and emitter dipole.

we neglect high frequency components  $\omega > > \omega_m$  that are filtered by microcantilever, since they do not produce any mechanical response on it, it is derived that the electrostatic force has, in this case, frequency components at  $\omega = 0$  (DC),  $\omega = \omega_m$  and  $\omega = 2\omega_m$ , yielding Eq. (11):

$$F_{ee,DC+AC} = \frac{\epsilon_0 \cdot A}{2 \cdot g_0^2} \cdot |V_m|^2 \left[ \frac{1}{2} + \frac{m^2}{4} + m \sin(\omega_m \cdot t) + \frac{m^2}{4} \cos(2\omega_m \cdot t) \right] \quad (11)$$

Consequently, when the frequency of the modulating signal  $\omega_m$  or twice this frequency,  $2\omega_m$  is tuned at the frequency of one of the vibration modes of the microcantilever, it is excited to resonate at one of these modes. The effect of these AC forces on the microcantilever predicted by the model are presented in Fig. 4, which shows the deflection of the MEMSTENNA,  $z(t)$ , when the emitter dipole has been excited by a carrier signal of frequency  $f_c = 531$  MHz, AM-modulated by a modulation signal of frequency  $f_m = 17$  kHz and  $f_m = 34$  kHz.

### 3. Measurement setup

The experimental measurements were performed using the setup shown in Fig. 5. The dipole antenna of the MEMSTENNA prototype and the emitter dipole antenna (ED) are placed in parallel at a distance,  $d$ . Both antennas have the same physical characteristics, resonance frequency, dimensions and  $S_{11}$  response as shown in Fig. 6. The MEMSTENNA is placed inside the vacuum chamber and the ED outside of it. Although the response of the antenna (Fig. 6) shows a maximum absorbed power peak at 0.8 GHz, the maximum coupling between antennas is achieved at  $f_c = 557$  MHz. This is because the two antennas are not perfectly identical and the MEMSTENNA cantilever loading will shift its resonance frequency. In addition, reflections on the vacuum chamber metal walls will modify the MEMSTENNA frequency response too. The emitter dipole ED is driven by an AM-modulated signal whose carrier is generated by a HP8647A signal generator and whose modulating signal is generated by the output of an Agilent 5061B Network Analyser. The modulated signal is amplified by a 2 W RF amplifier. The mechanical vibrations of the MEMSTENNA's microcantilever are detected by a conventional AFM-like optical readout system based on a red diode laser (RL) coupled to a 4-quadrant photodetector (4QPD). The readout signal obtained from the output of the photodetector is analysed in frequency through the Agilent 5061B Network Analyzer. A standard optical microscope configuration consisting of a 50X long working distance microscope objective (MO: Mitutoyo M Plan APO SL50X NA=0.42) and a CCD camera with paraxial illumination through a white light source (WLS) and a beam splitter (BS) is used to focus the red laser at the tip of the microcantilever.

### 4. Test results

Once the coupling between the emitter dipole and the MEMSTENNA has been maximized, the frequency response of the MEMSTENNA vibration amplitude of the first mechanical mode at different inter-antenna distances,  $d$ , is obtained by exciting with an amplitude modulated signal whose carrier frequency is  $f_c = 557$  MHz and sweeping the modulating frequency,  $f_m$ , around the first resonance mode, under

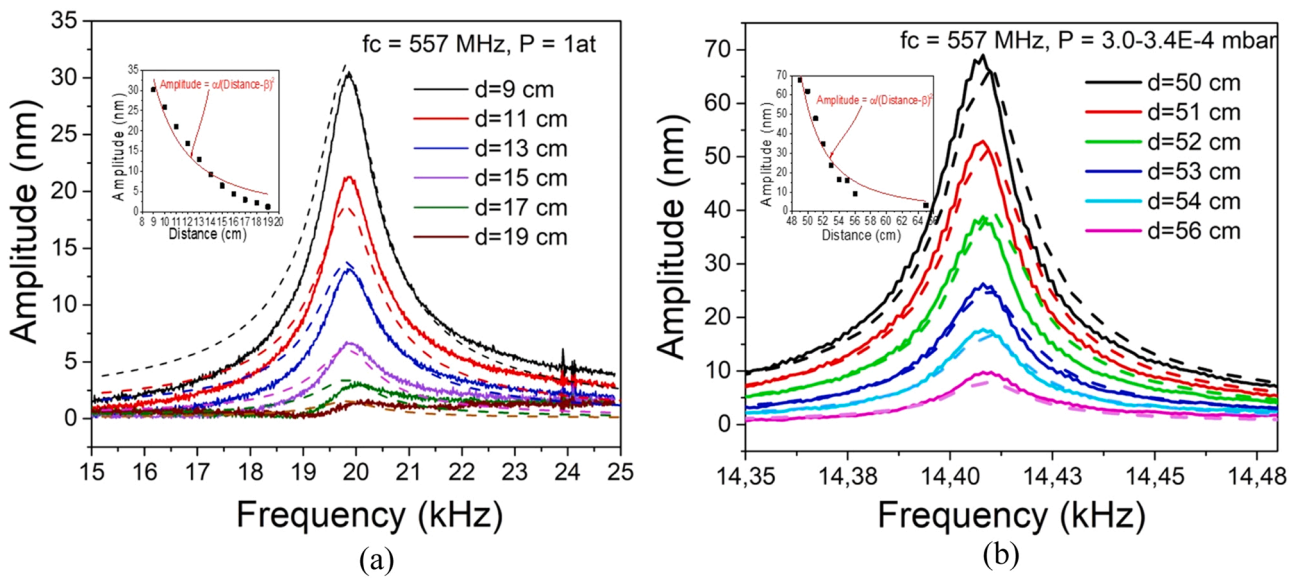


**Fig. 7.** Experimental frequency response of the MEMSTENNA's microcantilever vibration amplitude excited by an AM-modulated signal in air (a) and vacuum (b) (solid curves) together with the corresponding calculated predicted response (dash curves). In the insets, the peak amplitude values as a function of the inter-antenna distance,  $d$ , are represented along with their corresponding  $1/d^2$  fit curves.

vacuum and atmospheric pressure conditions, as shown in Fig. 7a and b, respectively. As shown in Fig. 7, the experimental resonant frequency measured value in air conditions was found to be 19.85 kHz. At this frequency the vibration peak amplitude detected by the photodetector was measured to be 30 nm. In vacuum conditions the experimental resonant frequency measured value was 14.405 kHz and the corresponding detected vibration peak amplitude was 68 nm. The measurements at atmospheric pressure are performed within the range of 9–19 cm, which corresponds to the radiating near field zone as defined in [32]. For  $f = 557$  MHz, the boundary between Reactive near fields and Radiating near-fields is, for a short dipole,  $\lambda/2\pi = 0.0857$  m. From the  $d = 9$  cm curve, the obtained values of the maximum vibration amplitude and quality factor are 32 nm and 20 respectively in air conditions.

When increasing the distance between antennas,  $d$ , the received power decreases by a factor of  $1/d^2$ . To analyse the response of the microcantilever at distances close to the far field regime, where for very small antennas the far field or Fraunhofer region is defined for a distance  $d_1 \approx 2\lambda$  [32], the pressure of the vacuum chamber enclosing the MEMSTENNA is pumped down, increasing the quality factor of the microcantilever to  $Q = 960$ . The maximum vibration amplitude of the microcantilever is also increased to 70 nm despite the fact that the inter-antenna distance is also increased up to 50 cm, which corresponds to  $d \approx \lambda$ , meaning that the system is in a transition zone between near and far field.

Inset of Fig. 7a and b show that the vibration amplitude of the microcantilever of the MEMSTENNA decays by a factor of  $1/d^2$  as expected, considering that the exciting electric field will decay according to the same trend as well.

Interestingly, we have found that the resonance frequency shifts down when pressure is decreased from air conditions ( $f_{\text{res}} = 19.9$  kHz) to vacuum ( $f_{\text{res}} = 14.405$  kHz). Such effect, which cannot be explained by the direct dependence of resonance frequency on the quality factor,  $f_{\text{res}} = f_0(1 - 1/2Q^2)^{1/2}$ , being  $f_0$  the undamped resonance frequency [31]. Effectively, as reported previously [24], the MEMSTENNA temperature in vacuum is higher than in air, since heat induced in the antenna by the joule effect produced when excited by the RF signal is evacuated much less efficiently in vacuum than in air conditions.

## 5. Conclusions

In summary, an electromechanical model of a MEMSTENNA device based on a folded-end dipole antenna and a commercial microcantilever has been presented. A test prototype has been built in order to characterize the mechanical dynamic response of the microcantilever to a remote excitation of the MEMSTENNA using an AM-modulated RF radiated signal, for different distances between the transmitting and receiving antennas, which cover from the near field to the transition zone between near and far field. Measurements performed with the MEMSTENNA into a vacuum chamber show that the increase of its Q-factor to 960 allows to extend the distances between antennas up to  $d \approx \lambda = 0.5$  m, and at the same time, it also allows for an increase in the amplitude of oscillation up to 70 nm. The electromechanical model has been validated with the experimental data obtained from test measurements using a RF-AM signal with a 557 MHz carrier frequency and a modulator frequency in the range of the mechanical frequency of the cantilever.

## Declaration of Competing Interest

The authors declare that they have no known competing financial interests or personal relationships that could have appeared to influence the work reported in this paper.

## Data Availability

Data will be made available on request.

## Acknowledgements

We would like to acknowledge Prof. Jordi Bonache and Dr. Ferran Paredes for their unvaluable scientific support and guidance through the microwave and antenna technologies. We would also like to acknowledge the financial support by Spain's Ministerio de Ciencia, Innovación y Universidades under Grant No. RTI2018-097876-B-C21 (MCIU/AEI/FEDER, UE).

## References

[1] N. Tesla, Electrical Transmission of Power, U.S. patent 511,915 Jan. 10, 1894.

[2] H. Yagi, S. Uda, 'On the feasibility of power transmission by electric waves', *Proc. 3rd Pan-Pac. Sci. Congr. Vol. 2* (1926) 1307–1313.

[3] J. Kim, H. Kim, D. Kim, D. Jeong, S. Ahn, "Analysis of Efficiency According to the Design of Transmitter Coil for Wireless Power Transfer Implantable Medical Device," 2020 IEEE Wireless Power Transfer Conference (WPTC), 2020, pp. 312–314, doi: 10.1109/WPTC48563.2020.9295618.

[4] A. Costanzo et al. , Wireless power transfer for wearable and implantable devices: a review focusing on the WPT4WID research project of national relevance 2021 XXXIVth Gen. Assem. Sci. Symp. . Int. Union Radio Sci. (URSI GASS) 2021 1 4 doi: 10.23919/URSIGASS51995.2021.9560425.

[5] M. Han, J.-M. Kim, H. Sohn, Dual-mode wireless power transfer module for smartphone application," 2015 IEEE International Symposium on Antennas and Propagation & USNC/URSI National Radio Science Meeting, 2015, pp. 111–112, doi: 10.1109/APS.2015.7304441.

[6] S.Y. Hui, Planar wireless charging technology for portable electronic products and Qi, Proc. IEEE vol. 101 (6) (2013) 1290–1301, <https://doi.org/10.1109/JPROC.2013.2246531>.

[7] S.-W. Dong , X. Li , X. Yu , Y. Dona , H. Cui , T. Cui , Y. Wang , S. Liu , Hybrid mode wireless power transfer for wireless sensor network 2019 IEEE Wirel. Power Transf. Conf. (WPTC) 2019 561 564 doi: 10.1109/WPTC45513.2019.9055665.

[8] S. Kuramoto , K. Akatsu , Basic experiment on high power transmission at 13.56MHz wireless power transfer for electric vehicle 2019 IEEE Veh. Power Propuls. Conf. (VPPC) 2019 1 5 doi: 10.1109/VPPC46532.2019.8952531.

[9] P.S. Yedavalli, T. Riihonen, X. Wang, J.M. Rabaey, Far-field RF wireless power transfer with blind adaptive beamforming for internet of things devices, *IEEE Access* vol. 5 (2017) 1743–1752, <https://doi.org/10.1109/ACCESS.2017.2666299>.

[10] S. Bellal, H. Takhedmit , L. Cirio , Design and experiments of transparent rectennas for wireless power harvesting 2016 IEEE Wirel. Power Transf. Conf. (WPTC) 2016 1 4 doi: 10.1109/WPT.2016.7498848.

[11] X. Gu, S. Hemour, K. Wu, Far-field wireless power harvesting: nonlinear modeling, rectenna design, and emerging applications, Proc. IEEE vol. 110 (1) (2022) 56–73, <https://doi.org/10.1109/JPROC.2021.3127930> (Jan).

[12] M. Donelli , J. Iannacci , Exploitation of RF-MEMS switches for the design of broadband modulated scattering technique wireless sensors *IEEE Antennas Wirel. Propag. Lett.* vol. 18 1 2019 44 48 doi: 10.1109/LAWP.2018.2880420.

[13] Eun-Chul Park , Taek-Sang Song , Sang-Hyun Baek , Euisil Yoon Low phase noise CMOS distributed oscillators using MEMS low loss transmission lines 17th IEEE Int. Conf. Micro Electro Mech. Syst. Maastricht MEMS 2004 Tech. Dig. 2004 645 648 doi: 10.1109/MEMS.2004.1290667.

[14] I.C. Reines, et al., A low loss RF MEMS Ku-band integrated switched filter bank, *IEEE Microw. Wirel. Compon. Lett.* vol. 15 (2) (2005) 74–76, <https://doi.org/10.1109/LMWC.2004.842823>.

[15] A.T. Alastalo, M. Koskenvuori, H. Seppa, J. Dekker, "A micro mechanical resonating RF mixer", 34th European Microwave Conference, Amsterdam, Netherlands, Vol. 3, pp. 1297–1300, 2004.

[16] Ark-Chew Wong, C.T.-C. Nguyen, Micromechanical mixer-filters ("mixlers"), *J. Micro Syst.* vol. 13 (1) (2004) 100–112, <https://doi.org/10.1109/JMEMS.2003.823218>.

[17] S. Chung, E.M. Abdel-Rahman, J. Yeow, "A MEMS Analog demodulator," IECON 2012 - 38th Annual Conference on IEEE Industrial Electronics Society, 2012, pp. 3946–3951, doi: 10.1109/IECON.2012.6389261.

[18] S. Park, E.M. Abdel-Rahman, "Low Voltage Electrostatic Actuation and Displacement Measurement through a Resonant Drive Circuit, ASME IDETC/CIE, August 2012, Chicago, IL, DETC2012-71268.

[19] Hao Yan, Xiaoping Liao, Chenglin Li, Chen Chen, A Cascaded MEMS amplitude demodulator for large dynamic range application in RF receiver, *Micromachines* 12 (2021) 1515, <https://doi.org/10.3390/mi12121515>.

[20] K. Jensen, J. Weldon, H. Garcia, A. Zettl, Nanotube radio, *Nano Lett.* 7 (11) (2007) 3508–3511. Nov 14.

[21] G. Abadal, P. Bramon, M. López-Suárez, J. Agustí, F. Torres, A microcantilever mechanical antenna, *Appl. Phys. Lett.* 115 (8) (2019), 083902. Aug 19.

[22] Ruiz R., Bonache J., Abadal G.. A flexible dipole antenna for direct transduction of microwave radiated power into DC mechanical deflection. Accepted in Sensors & Actuators A Physical.

[23] C. Belacel, Y. Todorov, S. Barbieri, D. Gacemi, I. Favero, C. Sirtori, Optomechanical terahertz detection with single meta-atom resonator, *Nat. Commun.* 8 (1) (2017) 1–8.

[24] Ruiz R., Abadal G.. Direct Transduction From Radiofrequency Radiated Power to Static and Dynamic Flexural Mechanical Modes. In 2021 21st International Conference on Solid-State Sensors, Actuators and Microsystems (Transducers) 2021 Jun 20 (pp. 144–147). IEEE.

[25] F. Huttu , A. Khoumri , G. Villemaud , J. Gorce , Wake-up radio architecture for home wireless networks 2014 IEEE Radio Wirel. Symp. . (RWS) 2014 256 258 doi: 10.1109/RWS.2014.6830103.

[26] A. Frøytag , L.R. Cenkeramaddi , Design and Implementation of an ultra-low power wake-up radio for wireless IoT Devices 2018 IEEE Int. Conf. Adv. Netw. Telecommun. Syst. (ANTS) 2018 1 4 doi: 10.1109/ANTS.2018.8710086.

[27] J.H. Hyun , L. Huang , D.S. Ha , Vibration and thermal energy harvesting system for automobiles with impedance matching and wake-up 2018 IEEE Int. Symp. . Circuits Syst. (ISCAS) 2018 1 5 doi: 10.1109/ISCAS.2018.8351419.

[28] NanoWorldTM Pirex Nitride AFM probe: PNP-TR-TL. (<https://www.nanoandmore.com>).

[29] O. Losito, et al., Antenna factor determination with Antenna Impedance measurements, *Int. Symp. . Electromagn. Compat. - EMC EUROPE* (2012) 1–4, <https://doi.org/10.1109/EMCEurope.2012.6396668>.

[30] V. Kaajakari, M.E.M.S. Practical, Design of microsystems, accelerometers, gyroscopes, RF MEMS, Opt. MEMS, Microfluid. Syst. (2009) (Small Gear, Estados Unidos).

[31] F. Aguilar Sandoval, M. Geitner, É. Bertin, L. Bellon, Resonance frequency shift of strongly heated micro-cantilevers, *J. Appl. Phys.* 117 (23) (2015), 234503.

[32] C.A. Balanis, *Antenna Theory. Analysis and Design*, John Wiley & Sons, New Jersey, 2005, 2.2, 2.5, 2.8, 3.2, 4.1.

**Raul Ruiz** received his M.S in Electronic Engineering in 2000 from the Universitat Autònoma de Barcelona. He has more than 18 years of experience in tasks of design and verification of ASIC. At present he works at EKRAN SYSTEMS as ASIC/SoC consulting engineer. His research interests include design, characterization and integration of micro and nanoelectromechanical systems (MEMS and NEMS). He is currently developing his PhD in MEMS direct transduction from electromagnetic to mechanical domain

**Dr. Gabriel Abadal** received his degree in physics in 1991 and his PhD in electrical engineering in 1997 from the UAB. Since 2002 he is an Associate Professor in the Electronics Engineering Department of the UAB, where he currently leads the NANERG LAB group (<http://grupsderecerca.uab.cat/nanerglab/>). During the last 28 years he has participated in more than 30 national and European research projects, he has contributed to more than 160 conferences and he has published more than 80 papers in journals (H-index: 21). Since 2006, he focused his activity in the application of MOEMS and NOEMS to harvest energy from ambient vibrations and electromagnetic radiation sources at the nanoscale. His actual interest is oriented towards the study of graphene and other 2D materials as basic components of the future nanoenergy harvesting strategies.